HHS Public Access

Author manuscript

Biomaterials. Author manuscript; available in PMC 2021 May 01.

Published in final edited form as:

Biomaterials. 2020 May ; 240: 119838. doi:10.1016/j.biomaterials.2020.119838.

A multilayered valve leaflet promotes cell-laden collagen type I production and aortic valve hemodynamics

Aline L.Y. Nachlas[a,+], **Siyi Li**[a,+], **Benjamin W. Streeter**[a], **Kenneth J De Jesus Morales**[a], **Fatiesa Sulejmani**[a], **David Immanuel Madukauwa-David**[c,d], **Donald Bejleri**[a], **Wei Sun**[a], **Ajit P. Yoganathan**[a], **Michael E. Davis**[a,b,*]

[a]Wallace H Coulter Department of Biomedical Engineering, Emory University and Georgia Institute of Technology, Atlanta, GA, USA

[b]Children's Heart Research & Outcomes (HeRO) Center, Children's Healthcare of Atlanta & Emory University, Atlanta, GA, USA

[c]Bioengineering Graduate Program, Georgia Institute of Technology, Atlanta, GA, USA

[d]George W. Woodruff School of Mechanical Engineering, Georgia Institute of Technology, Atlanta, GA, USA

Abstract

Patients with aortic heart valve disease are limited to valve replacements that lack the ability to grow and remodel. This presents a major challenge for pediatric patients who require a valve capable of somatic growth and at a smaller size. A patient-specific heart valve capable of growth and remodeling while maintaining proper valve function would address this major issue. Here, we recreate the native valve leaflet structure composed of poly-s-caprolactone (PCL) and cell-laden gelatin-methacrylate/poly(ethylene glycol) diacrylate (GelMA/PEGDA) hydrogels using 3D printing and molding, and then evaluate the ability of the multilayered scaffold to produce collagen matrix under physiological shear stress conditions. We also characterized the valve hemodynamics under aortic physiological flow conditions. The valve's fibrosa layer was replicated by 3D printing PCL in a circumferential direction similar to collagen alignment in the native leaflet, and GelMA/PEGDA sustained and promoted cell viability in the spongiosa/ventricularis layers. We found that collagen type I production can be increased in the multilayered scaffold when it is exposed to pulsatile shear stress conditions over static conditions. When the PCL component was mounted onto a valve ring and tested under physiological aortic valve conditions, the hemodynamics were comparable to commercially available valves. Our results

[*]**Address for correspondence:** Michael E. Davis, Ph.D., Professor, Department of Biomedical Engineering, Emory University and Georgia Institute of Technology, Health Science Research Building, 1760 Haygood Drive, Suite W200, Atlanta, GA 30322, Phone: 404-727-9858, michael.davis@bme.emory.edu.

[+]These authors contributed equally to this work.

Declaration of interests

The authors declare that they have no known competing financial interests or personal relationships that could have appeared to influence the work reported in this paper.

demonstrate that a structurally representative valve leaflet can be generated using 3D printing and that the PCL layer of the leaflet can sustain proper valve function under physiological aortic valve conditions.

2. Introduction

An estimated two to three million children live with heart disease, about 5% of whom have heart valve disease [1–3]. This is mainly due to congenital heart defects in industrialized countries and the persistence of rheumatic fever in underdeveloped regions [4–6]. Valve disease can be treated by valve replacement or repair. In most cases, valve repair is not possible, and valve implants have a number of risks, such as thrombogenicity and calcification. A significant issue for pediatric patients is the lack of small implants capable of growing, often requiring several surgical interventions for valve refitting [1,7]. Tissue engineered heart valves (TEHVs) have the potential to address limitations with current implants through their self-repairing and remodeling capacity.

Although there have been recent advancements in the field of TEHVs, developing a mechanically functional aortic TEHV for long-term implantation remains a challenge. Ideally, a TEHV should be biocompatible, durable, and anti-thrombogenic, and have a physiological hemodynamic profile. To date, a TEHV that meets all these criteria and can function under physiological aortic conditions has yet to be created.

The aortic heart valve opens and closes approximately four million times a year, with minimal transvalvular pressure gradients [7]. The mechanical strength of valves is attributed to the unique microstructure of each leaflet layer. The orientation of the extracellular matrix (ECM) of these layers is believed to enable the constant loading and unloading of the valve leaflets [8]. A challenge with tissue engineering an aortic valve is the difficulty in replicating the trilayer leaflet structure, which is comprised of the fibrosa, spongiosa, and ventricularis [7,9,10]. The fibrosa provides mechanical strength through circumferentially aligned collagen fibers. The spongiosa is the middle layer, rich in glycosaminoglycans, while the ventricularis is composed of radially aligned elastin. The leaflet layers are surrounded by valvular interstitial cells (VICs) which are responsible for maintaining the tissue homeostasis of the valve[8]. With the native valve leaflet structure and function as a guide, the goal is to design a scaffold that closely mimics this structure to develop a functional aortic TEHV.

To generate a functional TEHV, human induced mesenchymal stem cells (iMSCs) will be incorporated into the scaffold to promote matrix production. iMSCs were previously derived from induced pluripotent stem cells (iPSCs) and are patient-specific [11]. These cells, developed by our group[11], demonstrate VIC-like phenotype, characterized by low to minimal expression of alpha smooth muscle actin (aSMA) and positive expression of vimentin. They also have the capacity to produce collagen type I after encapsulation into PEGDA hydrogels. iMSCs have similar characteristics to VICs, which are known for their several sub-phenotypes ranging from mesenchymal stem cells to fibroblast-like cells and in some cases of disease osteoblast-like phenotypes[12]. The objective of this study is to provide an ideal microenvironment for the iMSCs to remain in a quiescent VIC-like stage described by low levels of aSMA and higher levels of vimentin expression and matrix production.

To create a mechanically functional TEHV, the biomaterials and the approach used are important. The biomaterial requirements for our TEHV are the ability to support cells, promote a physiological phenotype and cellular function, be compatible with 3D bioprinting, have tunable mechanical properties, and most importantly, undergo slow degradation over time. Considering these requirements, we have opted for two types of biomaterials: biodegradable poly-ε-caprolactone (PCL) and a formulation of gelatin methacrylate (GelMA) and polyethylene diacrylate (PEGDA). These two groups could enable us to incorporate cells into the leaflet scaffold, and these materials are compatible with 3D printing, allowing us to mimic the valve leaflet layers. Since the geometry and design are key components for a functional TEHV, 3D bioprinting and molding will be the primary approach used.

While other methods have been used to generate heart valve conduits, these approaches have been limited in their flexibility to utilize different materials in customized patterns, while enabling spatial placement of cells within each layer. Another major advantage of 3D printing is the ability to easily generate patient-specific valves of different geometries and sizes. The concept of using 3D bioprinting to generate a TEHV has been tested by various other groups [13,14]; however, the combination of biomaterials, geometry, and valve design has not yet been investigated and is hypothesized to enable the next generation of 3D bioprinted heart valves.

The objective of this study is to develop a multilayered valve leaflet using PCL and a GelMA/PEGDA bioink to generate a mechanically functional aortic TEHV that has the ability to promote a VIC-like phenotype and collagen type I production by the encapsulated cells while undergoing slow degradation. We hypothesize that a leaflet composed of 3D printed PCL and a hydrogel layer can be combined in a specific spatial orientation to recapitulate the ECM orientation observed in native leaflets, and that under physiological shear conditions, leaflets will have positive expression of VIC markers and demonstrate initial collagen type I production. When tested under aortic hemodynamic conditions, we hypothesize the PCL layer of the leaflet will sustain proper valve function similar to commercially available valve implants.

3. Methods and Materials

The method section is categorized into four sections: PCL, hydrogel, multilayered valve leaflet, and PCL heart valve. The order follows the process in which experiments were conducted. Note that all media components were purchased from Thermo Fisher Scientific unless otherwise stated. The time points day 0, 1 , and 7 are abbreviated as D0, D1, and D7, respectively, and from here onwards.

3.1. Cells

Human induced mesenchymal stem cells (iMSCs) derived from a feeder-free induced pluripotent stem cell protocol were used for experiments [11]. Cells were maintained in iMSC media containing KO-DMEM, 2mM L-glutamine, 10% fetal bovine serum (Atlanta Biologics), 1% nonessential amino acids, and 1% penicillin and streptomycin. The media was changed every 2 days.

3.2. PCL: 3D printing

For this study, poly-ε-caprolactone (PCL; Sigma-Aldrich) of molecular weight of 80,000 Da was used. Scaffolds were 3D printed to a thickness of 40-50 μm using the EnvisionTEC 3D Bioplotter (Gladbeck, Germany). PCL pellets were first melted in the high temperature cartridge to 180°C for 20-30 minutes before starting a print. Once melted, the PCL was extruded out of the metal cartridge through a 22G stainless steel Luer lock needle tip (EnvisionTEC). Scaffolds of different sizes were 3D printed at 4.0 bar and at a speed of 1.0 mm/s. The inner pattern design of the PCL scaffolds was controlled by the strand orientation. For instance, the circumferentially (parallel to force) aligned scaffold had the bottom layer strands aligned at 90° and the top layer strands at 180°. Meanwhile, the radially (perpendicular to force) aligned scaffold consisted of the bottom layer at 180° and the top layer at 90°. The diagonal orientation was achieved by printing a bottom layer at 30° follow by the top layer at 150° (Supplementary figure 1). All orientations were 3D printed into dogbones for mechanical testing.

3.3. PCL: Uniaxial tensile testing

To perform uniaxial tensile testing, PCL scaffolds were 3D printed into dogbone specimens following the ASTM D1708 – 13 guidelines. The dogbone specimen was designed using SOLIDWORKS to have a total length of 37.5 mm, gauge length of 15 mm, and a width of 5.5 mm. The thickness of the PCL scaffolds ranged from 60 to 160 μm. For uniaxial testing, a sample size of 4–7 samples were tested. To characterize the degradation properties of PCL scaffolds, the dogbone scaffolds were scaled down by a factor of 1.5 and were maintained in PBS solution at 37°C for up to 8 months. The thickness of these samples ranged from 30 to 50 μm. The uniaxial tensile properties of degraded samples were tested at 0 and 8 months. A sample size of 3–6 samples was used. Degraded samples were compared to control samples from Day 0. Before uniaxial testing, graphite markers were placed along the gauge length of the samples and sandpaper was attached to the end of the dogbone specimen to enhance grip. Uniaxial testing was performed on the TestResources SM-500–294 with a 25 lb-f load cell at a rate of 12 mm/min and 8 mm/min for the dogbone with a 37.5 mm and 25 mm length, respectively. The testing speed was changed to maintain the same strain rate in order to ensure the comparability of results. The upper and lower tangent moduli (UTM and LTM) and the ultimate tensile strength and ultimate tensile strain (UTS and UTE) were determined using MATLAB code (MathWorks), as previously described[15]. For statistical analysis, samples that were normally distributed, an unpaired ordinary one-way ANOVA with Holm-Sidak's multiple comparisons test was used, while for samples not normally distributed, a Kruskal-Wallis ANOVA test with Dunn's multiple comparisons test was performed. The same approach was used for comparing the degraded PCL scaffolds at 0 and 8 months; however, an unpaired t-test or a Mann-Whitney test was used.

3.4. PCL: Surface treatment of PCL and cell metabolism assessment

The hydrophobicity of the PCL surface and its ability to crosslink with other biomaterials can be modulated by grafting hydrophilic poly(methacrylic acid) (PMAA) onto PCL via a modified two-step protocol [16]. After rinsing PCL scaffolds in ethanol and deionized water, samples are submerged in 30% hydrogen peroxide solution (Sigma-Aldrich) and exposed to

UV light at 37°C for 6 hours. Next, samples were rinsed with deionized water and placed into a 4% weight-to-volume (w/v) solution of methacrylic acid (MAA) in deionized water for 2 hours under UV exposure at 37°C. PCL-MAA scaffolds were then rinsed with deionized water for 24 hours before use. Cell compatibility and adhesion onto the PCL-MAA scaffolds was assessed using the alamarBlue assay and immunostaining (detailed below). The only difference is that for PCL only scaffolds, only VIC phenotype via immunostaining was assessed and the Olympus IX71 microscope was used. Using non-treated 12-well plates, iMSCs were seeded onto PCL-MAA scaffolds at a density of 25×10^3 cells/mL. After D1 and D7, samples were thoroughly rinsed in PBS and alamarBlue was added as 10% of the sample media volume and incubated at 37°C. A fluorescence excitation wavelength of 560 nm was used and the fluorescence emission was read at 590 nm using the BioTek Synergy 2 plate reader (BioTek Instruments). The fluorescence values recorded on D7 were normalized to D1. The following experimental groups were utilized: PCL-MAA, PCL only, and controls of media only with alamarBlue were used. After the alamarBlue assay, samples were rinsed with PBS and then fixed in paraformaldehyde for immunostaining. An unpaired t-test was used to compare between D1 and D7 for cell metabolism data. To quantify the percent of cells with positive aSMA and vimentin expression using immunostaining an ordinary one-way ANOVA and a Tukey's multiple comparison test was used.

3.5. Hydrogel: Formulation and fabrication

Poly(ethylene glycol) diacrylate (PEGDA; ESI BIO) of molecular weight 3400 Da and gelatin methacrylate (GelMA; Cellink) were used to make hydrogels. A prepolymer solution of 5% w/v PEGDA, 10 μM Eosin Y (Santa Cruz Biotechnology), 0.375% v/v 1-vinyl-2-pyrrolidinone (NVP; Sigma-Aldrich), and 1.5% v/v triethanolamine (TEOA; Sigma-Aldrich) was dissolved in PBS of 80% the total volume. The prepolymer solution was sterile-filtered using the Spin-X Tube Filter (Corning). Subsequently, 7.5% w/v sterile GelMA was added to the prepolymer solution and incubated at 37C for 30 minutes with periodic vortexing prior to use. Cells were added to the solution at a concentration of 5×10^6 cells/mL to complete the remaining 20% of the total volume. Hydrogels were made by sandwiching 15 μL of prepolymer solution between a hydrophobic glass slide and a cover slip suspended by thin silicone rubber spacers (McMaster Carr) of 0.381 mm thickness on each side. After assembly, the hydrogels were incubated at 4°C for 5 minutes and then crosslinked usin g a white-light source (LED Light; Braintree Scientific, Inc.) for 5 additional minutes. Hydrogels were removed from the glass with a spatula and placed in media.

3.6. Hydrogel: Rheology

Rheological assessment for mechanical properties and hydrogel degradation was conducted on blank hydrogels and cell-laden hydrogels (5×10^6 cells/mL) at the following time points: D1, D7, D14, D21, and D28. This assessment was performed on the Anton Paar MCR 302 stress-controlled rheometer with a 9 mm diameter, 2° measuring cone. The storage and loss m oduli of the hydrogels were measured using dynamic oscillatory strain and frequency sweeps. The hydrogels were loaded on the plate, and the cone was lowered to the thickness of the hydrogel. An initial strain amplitude sweep was performed at 1.59 Hz to determine the linear viscoelastic range of the samples. Oscillatory frequency sweeps between 0.08 to

4.8 Hz were performed to determine the storage and loss moduli at 1.6 Hz [17]. All samples consisted of 5-6 technical replicates.

3.7. Hydrogel: Cell Viability

Hydrogels were collected at D1 and D7 time points for assessment of cell viability. A dead control was created by collecting and incubating one hydrogel in 70% methanol for 30 minutes at 37°C. All hydrogels were first rinsed with PBS and stained with the Live/Dead™ assay, consisting of a solution of 10 μM calcein AM and 5 μM ethidium homodimer, for 25 minutes at 37°C. They were then collected, rinsed with PBS, and placed back in media. A total of four images were captured per hydrogel using confocal microscopy (Olympus FV100) and for each image a random x,y,z location within the hydrogel was assigned. Then, cell viability was quantified using an automated counter in CellProfiler. A total of 5 biological replicates were used with a minimum of 3 technical replicates in each set. A paired t-test was used to compare between D1 and D7 for cell viability.

3.8. Multilayered valve leaflet: Preparation and Assembly

3D printed PCL-MAA and GelMA/PEGDA bioink were combined in a multilayered scaffold for testing under pulsatile shear stress (PSS) conditions. For samples tested under PSS, PCL-MAA was cut into rectangular scaffolds of 12 x 14 mm dimension. Then, 8 pL of prepolymer GelMA/PEGDA bioink was added to the scaffold with silicone spacers (McMaster Carr) of 0.381 mm thickness. The spacers were used to control the thickness of the bioink. Then, a circular glass coverslip (18 mm diameter) treated with Rain-X® Original glass repellent (RainX) was placed on top of the bioink with the spacers on each side. Prepolymer solution contained crosslinking components as previously mentioned with a cell concentration of 5 x 10^6 cells/mL. Before crosslinking, samples were placed at 4°C for 5 minutes followed by white-light crosslinking for 5 minutes at 4°C. A hydrogel layer of GelMA/PEGDA bioink was added to the PCL-MAA scaffold using a silicone spacer of 58 x 14 x 0.350 mm, which was centered on the scaffold.

3.9. Multilayered valve leaflet: Pulsatile shear stress (PSS) testing

To study the multilayered scaffold and assess VIC phenotype and ECM production under shear stress, a cone-in-plate bioreactor was used as previously described [18]. Using this system, 9 multilayered samples were loaded into the cone-in-plate bioreactor and tested for up to D7 under PSS with constant flow of iMSC media throughout the bioreactor. Control samples were multilayered scaffolds at D0 and D7 static conditions. The media was changed halfway through experiment. The PSS profile reached a peak shear stress of 80 dynes/cm^2 with a cycle duration of 800 ms consisting of an acceleration and deceleration phase to represent the systole and diastole phases of the cardiac cycle [19]. A minimum of 3 biological samples were used.

3.10. Multilayered valve leaflet: Immunostaining

The VIC phenotype and collagen I production was characterized in the multilayered scaffolds by using immunofluorescence staining and confocal microscopy (Olympus FV1000). To stain the nucleus, 4′,6-Diamidine-2′-phenylindole dihydrochloride (DAPI,

Sigma-Aldrich) was used. Hydrogels were fixed with 4% v/v paraformaldehyde for 20 minutes, permeabilized with 0.2% Triton X-100, and incubated for 1-hour in 1% bovine serum albumin (BSA; Sigma-Aldrich). All incubations were performed at room temperature thus far. Hydrogels were stained for collagen type I, αSMA, and vimentin using primary antibodies at 4°C overnight: mouse anti-human collagen type I (1:100; Abcam), mouse anti-human aSMA (1:100; Abcam), rabbit antihuman vimentin (1:100; Santa Cruz biotechnology). The following secondary antibodies were used: goat antimouse Alexa Fluor 647 (1:200), and goat anti-mouse Alexa Fluor 488 (1:200). Blank and cell-laden hydrogels were stained with secondary-only antibody as a control.

The amount of fluorescence was quantified using CellProfiler 3.1.8, where images for each stain were used to quantify presence of either nuclei or the VIC marker using the IdentifyPrimaryObjects function. Afterwards, RelateObjects and FilterObjects were used to determine the number of cells positive with the VIC marker of interest. The percent of cells positive for the VIC marker was calculated using the calculateMath function. Collagen type I staining was quantified using a similar approach to that of VIC markers expression, the only difference being that the percent area of a 1024x1024 image was calculated rather than the percent of positive cells. A total of 3 biological samples were used, and a minimum of 6 images were taken from different x, y, and z locations on the PCL or the multilayered scaffolds.

For the shear stress studies, a Kruskal-Wallis ANOVA test with Dunn's multiple comparison test was used for comparing the percent of cells positive for vimentin expression. While, an unpaired one-way ANOVA with Holm-Sidak's multiple comparison test was used for comparing the percent area covered by collagen type I staining at different time points, and the percent of cells expressing positive staining for αSMA.

3.11. PCL heart valve: Aortic heart valve prototype

To build a heart valve prototype, the two components necessary are the valve stent and the valve leaflet. Using SOLIDWORKS, a valve stent of 17 mm inner diameter and 19 mm outer diameter was designed referencing Thubrikar's work [20]. The valve stent was 3D printed using the Stratasys Objet30 Pro and the following two materials: the Objet RGD875 (VeroBlackPlus; Stratasys) and the FullCure 705 (Support Resin; Stratasys). A single valve leaflet composed of PCL-MAA scaffold was attached to the valve stent via cyanoacrylate (Loctite® 404).

3.12. PCL heart valve: Hemodynamic profile of prototype

To determine the hemodynamics of the heart valve prototype, TEHVs were placed in a left-heart flow loop, previously detailed [21]. The simulator consists of four main components: flow, pressure, data acquisition, and flow visualization. Pressure and flow data were acquired at 1000 Hz over 100 simulated cardiac cycles with 3 technical repeats. Two cardiac outputs, 2.5 and 5 L/min, were evaluated using a water-glycerin mixture (36% glycerin), which recapitulates the kinematic viscosity of blood. Using previous methods [21,22], the following parameters were measured and/or computed: the mean transvalvular pressure gradient (TVPG), regurgitation volume, leakage volume, and the effective orifice area (EOA). The

duration of the valve opening during one cardiac cycle was assessed by determining the intersection of the ventricular and aortic pressures measured by the pressure probes fitted on the simulator. To image the valve dynamics, a slow-motion video at 240 frames per second was captured using an iPhone Xs. A total of 4 valves were tested under aortic valve flow and pressure conditions.

3.13. Statistical Analysis

All quantitative data were expressed as the mean ± standard deviation (SD). Statistical analysis was performed using Prism 8 (Graphpad) and all experiments were tested for normality using the Shapiro-Wilk test. For all experiments, unless otherwise stated, sample size n = 3-5 and technical replicates were used. Statistical significance was considered at a value of $p < 0.05$. Specific statistical analysis was detailed within each section of the methods.

4. Results

The results of this study describe the progression of developing the layers of the valve leaflet and testing the TEHV in physiological conditions. The first two steps were to individually develop and test the PCL and hydrogel layers of the valve leaflet. Then, the two layers were combined to develop the multilayered valve leaflet, which was studied under physiological shear stress conditions observed in the aortic valve. Lastly, a TEHV with the PCL layer of the leaflet was observed under physiological flow and pressure conditions as this is the load-bearing layer. The results are summarized under four categories as stated in the methods section and these are PCL, hydrogel, multilayered valve leaflet, and PCL heart valve.

4.1. PCL: Mechanical and degradation properties of PCL scaffold

To develop the fibrosa layer of the valve leaflet, PCL scaffolds were 3D printed in three fiber orientations (perpendicular, parallel, and diagonal) and evaluated using uniaxial tensile testing, as shown in Figure 1a. The representative Cauchy-Green stress-strain curve demonstrates a similar shape among the different fiber orientations, where there was a linearly elastic phase up to 7-12% Green strain, followed by a plastic deformation phase thereafter. In Figure 1a, the upper tangent modulus (UTM) and lower tangent modulus (LTM) were calculated for all three fiber orientations. The average UTM was 5.2 MPa for perpendicular fiber alignment, 3.7 MPa for the parallel fiber alignment, and 4.1 MPa for the diagonal fiber PCL scaffolds. The perpendicular scaffolds' UTM was statistically significant when compared to the parallel aligned scaffolds' UTM, and no significance was determined when compared to diagonal scaffolds' UTM. As for the LTM, no statistical significance was determined among all three alignments, and the average LTM was 139.8, 204.2, and 137.6 MPa for the perpendicular, parallel, and diagonal fiber directions, respectively. Furthermore, the ultimate tensile strength (UTS), which describes the maximum stress a material can withstand before failure, was the highest for the parallel aligned scaffolds at 168.1 MPa, while the perpendicular UTS was 155.2 MPa followed by 92.8 MPa for the diagonal scaffolds. There was no statistical difference between the perpendicular and parallel scaffolds; however, the diagonal scaffolds' UTS was statistically lower when compared to the parallel scaffolds' UTS. Lastly, the ultimate tensile elongation (UTE) for the parallel

scaffolds was significantly higher than that of the other two fiber orientations with a strain of 26.6, while perpendicular and diagonal scaffolds' UTE's were 19.7 and 14.8, respectively.

The mechanical properties of PCL scaffolds of the perpendicular and parallel fiber orientations were assessed to determine changes in bulk properties due to degradation (Supplementary Figure 2). Perpendicular PCL scaffolds did not show evidence of degradation based on their UTM and LTM properties; however, there was a significant decrease in UTS and UTE when comparing 0 to 8 months. The UTS significantly decreased from 155.2 MPa to 62 MPa after 8 months, while the UTE also significantly decreased from 19.7 MPa to 8.9 MPa. Meanwhile, parallel scaffolds experienced a significant increase in the UTM between 0 and 8 months, where the UTM increased from 3.7 MPa to 5.1 MPa. As for the LTM, UTS, and UTE, no changes in the material's properties were observed at 0 and 8 months.

4.2. PCL: Characterization of iMSC phenotype and metabolism when seeded on PCL-MAA scaffolds

To generate a multilayered scaffold composed of both the PCL scaffold (circumferentially aligned) and the GelMA/PEGDA hydrogel, the hydrophobicity of the PCL was modulated by grafting hydrophilic methacrylic acid (MAA). After surface modification the cell phenotype and metabolism of iMSCs were assessed on the PCL-MAA scaffold. The effects of the PCL-MAA or PCL scaffold on iMSC phenotype were characterized via αSMA and vimentin immunostaining and quantification of percent positive cells for each marker. Tissue culture (TC) was used as a control. For αSMA staining, there were 27.6, 34.4, and 54.3% positive cells when seeded on PCL-MAA, PCL, and TC, respectively, with no statistical significance between scaffolds. Meanwhile, 63.1% and 62.6% of iMSCs stained positive for vimentin when seeded on PCL-MAA and PCL, respectively, whereas, 24.1% of the cells seeded on tissue culture (TC) plates expressed vimentin. iMSCs seeded on PCL-MAA scaffolds had positive diffuse staining of vimentin in most of the cells, with a few cells staining for αSMA stress fibers. Cells seeded on the PCL-only scaffold also had diffuse staining of vimentin, except cells did not demonstrate distinct stress fibers of αSMA and rather had αSMA staining at the focal adhesion sites. On the TC plate, iMSCs showed minimal staining of vimentin and staining of very distinct stress fibers of αSMA. Next, the cellular health and metabolic function of iMSCs seeded on both PCL-MAA and PCL scaffolds were assessed using alamarBlue, at D1 and D7 as shown in Figure 2f. The level of fluorescence was normalized to D1 and then compared between the two samples. Fluorescence of PCL scaffolds treated with methacrylic acid (PCL-MAA) was statistically higher than that of PCL scaffolds, with four times more fluorescence.

4.3. Hydrogel: Mechanical properties and cell viability of iMSCs encapsulated in GelMA/PEGDA hydrogels

For the spongiosa and ventricularis layer of the valve leaflet, we used a combination of GelMA and PEGDA hydrogels. It was important to characterize the mechanical properties of cell-laden hydrogels to ensure the properties are representative of what native cells experience within the leaflets. The mechanical properties were also used as a measure of degradation over the course of 28 days. The storage and loss moduli of blank hydrogels and

cell-laden hydrogels were measured over a range of frequencies, as shown in Supplemental Figure 3, and measurements taken at 1.6 Hz were compared across groups, as shown in Figure 3. The storage moduli of blank and cell-laden hydrogels indicated a significant difference, with cell-laden hydrogels exhibiting a lower storage modulus on average compared to that of blank hydrogels. However, comparisons of storage moduli across 28 days showed no significant changes in either experimental group. Similarly, a significant decrease in loss modulus was also observed between blank and cell-laden hydrogels. In the loss moduli, the majority of time points did not significantly differ over time, with the only exception being between D7 and D28 for blank hydrogels. Evaluating cell viability within these hydrogels is important to ensure that they are able to produce ECM components to remodel and regenerate the leaflet. As shown in Figure 3c–e, iMSCs encapsulated in 7.5% w/v GelMA and 5% w/v PEGDA hydrogels remained viable at 92% at D1. By D7, iMSC viability decreased to 80%. While the decrease from D1 to D7 was significant, encapsulated iMSCs remained viable within the hydrogels.

4.4. Multilayered valve leaflet: VIC phenotype and collagen type I production.

The expression of αSMA and vimentin was quantified and compared between D0, D7 static, and D7 PSS (Figure 4). In the multilayered scaffolds, 12% of encapsulated cells were positive for αSMA at D0. Under static conditions at D7, an average of 25% of cells were positive for αSMA. While scaffolds under PSS conditions, had an average of 23% of the cells positively expressing αSMA. When staining for vimentin, 7.7%, 7.3%, and 27.9% of the cells expressed vimentin in the multilayered scaffolds at D0, D7 static, and D7 PSS, respectively. There was no statistical difference between time points or different culture conditions for both αSMA and vimentin expression. Representative images of the immunostaining of αSMA and vimentin are demonstrated in Figure 4 c–e. At D0 and D7 static conditions, there is diffuse staining of αSMA, while cells have a combination of diffuse and punctate staining of vimentin and punctate staining of αSMA after 7 days of PSS conditions. No evidence of background staining was present in the 2° antibody only images for αSMA and vimentin (data not Collagen type I deposits were also quantified through immunostaining and compared between D0, D7 static, and D7 PSS in Figure 5. At D0, there was minimal evidence of collagen type I. Under static conditions, there was an increase in collagen deposition by D7 at an average of 0.15% of the total imaged area. Multilayered scaffolds exposed to PSS for 7 days exhibited 0.34% of the imaged area as positive for collagen type I, which was statistically higher compared to D7 static conditions. The increase in collagen type I area in both the 7-day time points was determined to be statistically higher when compared to that of D0. In Figure 5b, immunostaining demonstrated minimal to no staining of collagen type I. At D7 under static and PSS conditions, there was diffuse collagen type I staining surrounding the cells. In control samples stained only with 2nd antibody, no collagen type I staining was observed (image not shown).

4.5. PCL heart valve: TEHV prototype design

To demonstrate the feasibility of using PCL as the load-bearing layer of the multilayered leaflet scaffold, a valve stent composed of three posts was developed using 3D printing. The valve stent had an inner diameter of 17 mm and a 19 mm outer diameter as shown in Figure

6a. In order to test in the flow loop, an additional outer ring (Figure 6b) was added to the valve stent for proper placement. The PCL leaflet was 3D printed with the parallel fiber orientation as shown in Figure 6c and when mounted it was circumferentially placed. Next, the leaflet was successfully wrapped around the valve stent using cyanoacrylate. The placement of the leaflet was measured to have an excess length of 2 mm above the valve post. In Figure 6 d,e the mounted PCL leaflet can be observed in an open and semi-closed state. This approach enabled consistency between valve prototypes and an average of 30-40 minutes assembling time.

4.6. PCL heart valve: TEHV hemodynamics

The hemodynamic profile of the TEHV was characterized using a pulsatile flow loop capable of mimicking physiological flow rates. The ventricular and aortic pressures were measured during the cardiac cycle (Figure 7a). Using these measurements, the duration of 0.18 ± 0.019 seconds for the TEHV-PCL to rapidly open and close during a cardiac cycle was observed. A side and cross-sectional view of the valve opening, and closing was captured in Figure 7b. Valves were inspected after hemodynamic testing and no visible deformation or damage was detected. Next, the hemodynamic profile of the TEHVs was characterized through three parameters: mean transvalvular pressure gradient (TVPG), changes in volume, and effective orifice area (EOA). In Figure 8a, the hemodynamics profile of the TEHV was assessed via the mean TVPG, which was 2.9 mm Hg for the 2.5L/min cardiac output and higher at an average of 10.4 mm Hg for the 5L/min cardiac output. As for the changes in volume, minimal regurgitation was detected for both cardiac outputs. The closing volume of the valve was 3.2- and 3.4 mL for the 2.5 L/min and 5L/min, respectively. Leakage volume was minimal for both cardiac outputs, with the maximum volume reaching 2.8 mL. The EOA was calculated to be 1.23 cm^2 at 2.5 L/min cardiac output, and at 5L/min the EOA was 1.41 cm^2.

5. Discussion

Heart valve tissue engineering has the potential to address the limitations of current mechanical and bioprosthetic heart valve implants. Most importantly, TEHVs could favorably impact the pediatric population, who currently rely on heart valve implants that were designed and made for adults. Here, our goal was to develop a multilayered valve leaflet using PCL and GelMA/PEGDA bioinks to generate a mechanically functional aortic TEHV that has the ability to promote healthy VIC-like phenotype and collagen type I production and is capable of degrading over time. Two steps were taken to engineer functional aortic TEHVs, where first, a rationally designed heart valve leaflet composed of both synthetic and natural polymers was developed, and second, the feasibility of using the manufactured heart valve leaflet in physiological aortic flow and pressure conditions was evaluated.

The heart valve leaflet was designed considering the structural and mechanical properties of the fibrosa layer in native leaflets, where the collagen fibers are circumferentially aligned, and the mechanical properties are anisotropic [23]. In this study, PCL was 3D printed in three different fiber orientations to determine which scaffold would yield mechanical properties

similar to that of native leaflets. The stress-strain curve of the PCL scaffolds was observed to have two phases with distinct tangent moduli and the shape of the curve suggests the scaffold is not relatively elastic. The UTMs of the PCL scaffolds in all three fiber orientations were within the physiological range of 4 – 13 MPa [24] with the perpendicular fiber's UTM statistically higher compared to that of the parallel orientation. This suggests that fiber orientation can produce anisotropy because at different orientations, a significant difference in the UTM was observed. At the UTM, it is important to notice the PCL scaffolds undergo plastic deformation. The LTM, regardless of the fiber orientation, was much higher than native tissue, where there was no statistical difference among the different fiber orientation LTMs. Given that native leaflets have a modulus of 4 – 13 MPa [24], it suggests that under physiological conditions it is unlikely that the PCL scaffolds will undergo any major deformation or fracture.

A possible reason for the two different tangent moduli observed with the 3D printed PCL scaffolds could be due to the manufacturing process used. PCL scaffolds were 3D printed using fibers of melted polymer which created crosslinking between fibers, yielding a very high initial tangent modulus. This can describe why we observe a stiffer material reinforced by the crosslinking of the fibers. Once the crosslinks have unlinked, we observe the true modulus, where the PCL scaffold is more compliant. The statistical difference between all three strand orientations for the UTE indicates that the introduction of different orientations can affect the overall UTE of the scaffold, which further suggests that strand orientation can introduce anisotropic properties to the scaffolds. Overall, PCL scaffolds have some resemblance to the native leaflet. For further studies, the parallel fiber aligned PCL scaffolds were investigated, as these fibers most closely resemble collagen fiber alignment when mounted on the valve stent. Given that we are engineering a TEHV that has the capacity to degrade and remodel over time, it was important to assess short-term degradation to ensure that this material would not degrade too quickly. Degradation of the PCL scaffolds is characterized to be slow and not evident in the UTM and LTM properties of the perpendicular fiber alignment. However, there was evidence of some degradation through the significant decrease in UTS and UTE for the perpendicular fiber orientation, suggesting that fiber orientation plays a role in the material properties. Evidence of degradation is to be expected for PCL as it has a slow degradation rate of 24-36-months [25]. As for the parallel fiber orientation, no statistical changes in the LTM, UTS, and UTE were observed, and unexpectedly, there was a very small increase in the UTM over 8 months in degradation conditions. This increase could be explained by instrumentation errors or variability in the samples. Future studies will involve studying how the variation in strand distribution and density between layers can further affect the anisotropic properties of our scaffold. In addition, the introduction of other biomaterials such as poly(glycerol sebacate) (PGS) can help modify the material properties of the scaffold to better match the native moduli of the valve leaflet [26].

Next, the PCL scaffold was surface treated with poyl(methacrylate acid) in order to reduce hydrophobicity and to ensure that this material can be crosslinked with the hydrogel biomaterial. The health of iMSC metabolism post-surface treatment was important to ensure cells interacting with the PCL remained viable and healthy. AlamarBlue data demonstrated that iMSCs have higher metabolic activity compared to PCL-only scaffolds, suggesting that

decreasing hydrophobicity led to more cellular metabolic activity. It could also suggest that more cells were able to adhere onto the PCL-MAA scaffold compared to PCL scaffolds. Previous studies have demonstrated that when hydrophobicity is decreased, more cell adhesion is observed [27]. Furthermore, it was important to characterize the VIC-like phenotype of iMSCs seeded on PCL-MAA scaffolds given the stiffness of PCL and its potential to elicit an activated myofibroblast-like phenotype. On average 35-40% of the iMSCs adhered on PCL scaffolds were positive for αSMA expression, regardless of MAA treatment. Interestingly, iMSCs were 50-60% positive for vimentin expression, suggesting that iMSCs, when seeded on PCL and PCL-MAA, are more VIC-like compared to TC control. If iMSCs remain activated through long-term expression of αSMA, an alternative is to utilize ascorbic acid to modulate the cell phenotype while promoting ECM remodeling [28].

The next component of the multilayered leaflet is the hydrogel-based bioink composed of GelMA/PEGDA. The degradation of this material is important to characterize as this material should ideally degrade slowly to enable cells to remodel and produce ECM. Overall, there was a significant difference in the storage and loss modulus between blank and cell-laden hydrogels. When cells are added to a matrix scaffold, previous studies have observed a decrease in compressive moduli compared to acellular scaffolds [29–31]. This could be explained by the cells' ability to partially absorb some of the loading forces and the impact they can have on the photopolymerization of the GelMA/PEGDA hydrogel [30]. Overall, no difference in moduli was observed over different time points suggesting low to minimal degradation of the GelMA/PEGDA hydrogels short-term. If necessary, slow matrix metalloproteinases (MMP) cleavable degradation peptides may need to be introduced into the GelMA/PEGDA bioink to control degradation [32]. The cell viability of iMSCs was assessed in cell-laden hydrogels of GelMA/PEGDA, and while there was a decrease in cell viability, 80% viability is considered acceptable for future experiments, thus suggesting that overall, the GelMA/PEGDA hydrogel is suitable for use in the valve leaflet.

The VIC-like phenotype and collagen type I production was studied in the multilayered scaffolds under pulsatile shear stress conditions for 7 days. To characterize iMSC phenotype and collagen type I deposition, scaffolds were immunostained for αSMA, vimentin, and collagen type I. We have previously shown that iMSCs in PEGDA hydrogels transition from an activated VIC-like phenotype to a more quiescent state, and that these cells have the capacity to produce collagen type I shortly after 7 days under static conditions [11]. Under PSS, we did not observe any changes in αSMA and vimentin expression, with 20% of cells positive for αSMA and vimentin. Results from immunostaining suggest that under PSS and in the multilayered scaffold, we did not observe an activated VIC-like phenotype nor expression of vimentin. It is worthwhile noticing that this was only D7 and that a longer time point may be necessary. While no changes in cell phenotype were observed, the amount of collagen type I produced was significantly higher at D7 under PSS compared to that of D7 static and D0. Furthermore, the diffuse staining appeared to be surrounding the cells suggesting that collagen type I production is possible under PSS and in the cell-laden multilayered leaflet scaffold. In addition to collagen type I, we also investigated the production of GAGs (supplementary figure 6) and did not observe an increase in either the static or PSS conditions. It is important to note that this study was limited by the duration of

the time points, which may not be sufficient to capture GAG production. Thus, future studies will investigate GAG production at longer time points.

While developing a multilayered leaflet capable of repairing and remodeling is important, it is just as essential to test whether this leaflet is capable of withstanding aortic valve flow and pressure conditions. Previous groups have developed TEHVs that function under pulmonic valve conditions [33–35]; however, to date only one TEHV has been capable of withstanding aortic conditions, which is an off-the-shelf decellularized TEHV [36]. Thus, the objective was to evaluate whether our rational design for the multilayered leaflet had the capacity to mechanically function under aortic physiological flow conditions. Here, only the PCL layer was tested under flow conditions and future studies will investigate the multilayered leaflet with the hydrogel layer. Ongoing studies are focused on the manufacturing assembly of the multilayered leaflet onto the valve stent with minimal to no damage to the hydrogel layer of the leaflet. Before testing, the PCL scaffold was assembled onto a valve stent with reproducibility. Under *in vitro* aortic valve conditions at 5L/min cardiac output, the TEHV-PCL had a lower mean TVPG at 10.4 mm Hg compared to previously reported values of 14.6- and 15 mm Hg for the St. Jude Medical Valve [37–39]. Furthermore, there were minimal changes to the regurgitation, closing, and leakage volumes suggesting the TEHVs were opening and closing properly. When compared to the St. Jude mechanical valve of 19 mm size, there was a decrease in regurgitant volume of 6.2 mL/beat in the TEHV-PCL valves from the 10.8 mL/beats of regurgitant volume in the St. Jude valve [37–39]. However, the TEHV-PCL valves did not decrease to the regurgitant volumes of less than 2 mL/beat as reported for the CarboMedics Mitroflow pericardial valve of 19 mm size [40]. In addition, the TEHV-PCL demonstrated an higher EOA of 1.41 cm^2 when compared to the EOA of St. Jude mechanical valve and the CarboMedics Mitroflow pericardial valve, which were 1.21 cm^2 and 1.34 cm^2, respectively [40]. While these are initial tests, the TEHV-PCL valve demonstrates promising hemodynamics results, and future studies will investigate the hemodynamic performance of the TEHV with the multilayered leaflet.

6. Conclusions

Most TEHVs have been developed for the pulmonary position as TEHVs capable of withstanding aortic valve conditions are required to be more durable. Here, we demonstrate a multilayered heart valve leaflet can be composed of 3D printed PCL and a hydrogel layer to recapitulate structural features of native leaflets. Each material used for the multilayered leaflet was assessed for its mechanical properties and its interactions with iMSCs to ensure that cells remained viable and maintained a healthy VIC-like phenotype. Furthermore, the multilayered leaflet under pulsatile shear stress conditions resulted in collagen type I production suggesting the leaflet is capable of ECM production over time. The PCL component of the multilayered leaflet was assembled into a valve stent to evaluate whether this layer of the TEHV, which was designed to be the load-bearing layer, can withstand aortic valve flow and pressure conditions. The hemodynamic studies demonstrate the TEHV has similar EOA and mean transvalvular pressure gradient to that of commercially available valves. While the TEHV is promising, future studies are necessary to evaluate the multilayered leaflet under aortic valve conditions as well as assess its growth and remodeling potential.

Supplementary Material

Refer to Web version on PubMed Central for supplementary material.

Acknowledgements

This work was supported by The Betkowski Family Research Fund, NSF Graduate Research Fellowship, American Heart Association Predoctoral Fellowship (award no. 16PRE31100011), NRSA NIH F31 Predoctoral fellowship (award no. 5F31HL136184-02), Alfred P. Sloan Foundation, Goizueta Foundation, and the PEO Scholar award to A.L.Y.N, and the Petit Scholar Program to S.L. This research project was supported in part by the Emory University Integrated Cellular Imaging Microscopy Core of the Emory+Children's Pediatric Research Center. Additional support was provided by the National Center for Advancing Translational Sciences of the National Institutes of Health under Award Number UL1TR000454. The content is solely the responsibility of the authors and does not necessarily reflect the official views of the National Institutes of Health.

REFERENCES

1. Henaine R, Roubertie F, Vergnat M & Ninet J Valve replacement in children: a challenge for a whole life. Arch Cardiovasc Dis 105, 517–528, doi:10.1016/j.acvd.2012.02.013 (2012). [PubMed: 23062483]
2. Detter C, Fischlein T, Feldmeier C, Nollert G & Reichart B Aortic valvotomy for congenital valvular aortic stenosis: a 37-year experience. Ann Thorac Surg 71, 1564–1571 (2001). [PubMed: 11383801]
3. Samanek M Congenital heart malformations: prevalence, severity, survival, and quality of life. Cardiology in the young 10, 179–185 (2000). [PubMed: 10824896]
4. Takkenberg JJ et al. The need for a global perspective on heart valve disease epidemiology. The SHVD working group on epidemiology of heart valve disease founding statement. J Heart Valve Dis 17, 135–139 (2008). [PubMed: 18365583]
5. Marijon E, Mirabel M, Celermajer DS & Jouven X Rheumatic heart disease. Lancet 379, 953–964, doi:10.1016/S0140-6736(11)61171-9 (2012). [PubMed: 22405798]
6. Writing Group, M. et al. Executive Summary: Heart Disease and Stroke Statistics--2016 Update: A Report From the American Heart Association. Circulation 133, 447–454, doi:10.1161/CIR.0000000000000366 (2016). [PubMed: 26811276]
7. Sacks MS, Schoen FJ & Mayer JE Bioengineering challenges for heart valve tissue engineering. Annual review of biomedical engineering 11,289–313, doi:10.1146/annurev-bioeng-061008-124903 (2009).
8. Chester AH et al. The living aortic valve: From molecules to function. *Global cardiology science & practice* 2014, 52–77, doi:10.5339/gcsp.2014.11 (2014). [PubMed: 25054122]
9. Balachandran K, Sucosky P & Yoganathan AP Hemodynamics and mechanobiology of aortic valve inflammation and calcification. International journal of inflammation 2011,263870, doi:10.4061/2011/263870 (2011). [PubMed: 21760982]
10. Cheung DY, Duan B & Butcher JT Current progress in tissue engineering of heart valves: multiscale problems, multiscale solutions. Expert Opin Biol Ther 15, 1155–1172, doi:10.1517/14712598.2015.1051527 (2015). [PubMed: 26027436]
11. Nachlas ALY et al. Human iPSC-derived mesenchymal stem cells encapsulated in PEGDA hydrogels mature into valve interstitial-like cells. Acta Biomater71, 235–246, doi:10.1016/j.actbio.2018.02.025 (2018). [PubMed: 29505894]
12. Liu AC, Joag VR & Gotlieb AI The emerging role of valve interstitial cell phenotypes in regulating heart valve pathobiology. Am J Pathol 171, 1407–1418, doi:10.2353/ajpath.2007.070251 (2007). [PubMed: 17823281]
13. Duan B, Hockaday LA, Kang KH & Butcher JT 3D bioprinting of heterogeneous aortic valve conduits with alginate/gelatin hydrogels. Journal of biomedical materials research. Part A 101, 1255–1264, doi:10.1002/jbm.a.34420 (2013). [PubMed: 23015540]
14. Jana S & Lerman A Bioprinting a cardiac valve. Biotechnol Adv 33, 1503–1521, doi:10.1016/j.biotechadv.2015.07.006 (2015). [PubMed: 26254880]

15. Pokutta-Paskaleva A, Sulejmani F, DelRocini M & Sun W Comparative mechanical, morphological, and microstructural characterization of porcine mitral and tricuspid leaflets and chordae tendineae. Acta Biomater 85, 241–252, doi:10.1016/j.actbio.2018.12.029 (2019). [PubMed: 30579963]
16. Zhu Y, Gao C & Shen J Surface modification of polycaprolactone with poly(methacrylic acid) and gelatin covalent immobilization for promoting its cytocompatibility. Biomaterials 23, 4889–4895 (2002). [PubMed: 12361630]
17. Bhutani S et al. Evaluation of Hydrogels Presenting Extracellular Matrix-Derived Adhesion Peptides and Encapsulating Cardiac Progenitor Cells for Cardiac Repair. ACS Biomater Sci Eng 4, 200–210, doi:10.1021/acsbiomaterials.7b00502 (2018). [PubMed: 29457128]
18. Sucosky P et al. Design of an ex vivo culture system to investigate the effects of shear stress on cardiovascular tissue. J Biomech Eng 130, 035001, doi:10.1115/1.2907753 (2008). [PubMed: 18532871]
19. Cao K & Sucosky P Computational comparison of regional stress and deformation characteristics in tricuspid and bicuspid aortic valve leaflets. Int J Numer Method Biomed Eng 33, doi:10.1002/cnm.2798 (2017).
20. Thubrikar M The aortic valve. (CRC Press, 1990).
21. Yap CH et al. Dynamic deformation characteristics of porcine aortic valve leaflet under normal and hypertensive conditions. Am J Physiol Heart Circ Physiol 298, H395–405, doi:10.1152/ajpheart.00040.2009 (2010). [PubMed: 19915178]
22. Leo HL, Dasi LP, Carberry J, Simon HA & Yoganathan AP Fluid dynamic assessment of three polymeric heart valves using particle image velocimetry. Ann Biomed Eng 34, 936–952, doi:10.1007/s10439-006-9117-5 (2006). [PubMed: 16783650]
23. Martin C & Sun W Biomechanical characterization of aortic valve tissue in humans and common animal models. Journal of biomedical materials research. Part A 100, 1591–1599, doi:10.1002/jbm.a.34099 (2012). [PubMed: 22447518]
24. Vesely I & Noseworthy R Micromechanics of the fibrosa and the ventricularis in aortic valve leaflets. J Biomech 25, 101–113 (1992). [PubMed: 1733978]
25. Sun H, Mei L, Song C, Cui X & Wang P The in vivo degradation, absorption and excretion of PCL-based implant. Biomaterials 27, 1735–1740, doi:10.1016/j.biomaterials.2005.09.019 (2006). [PubMed: 16198413]
26. Kemppainen JM & Hollister SJ Tailoring the mechanical properties of 3D-designed poly(glycerol sebacate) scaffolds for cartilage applications. Journal of biomedical materials research. Part A 94, 9–18, doi:10.1002/jbm.a.32653 (2010). [PubMed: 20091702]
27. Webb K, Hlady V & Tresco PA Relative importance of surface wettability and charged functional groups on NIH 3T3 fibroblast attachment, spreading, and cytoskeletal organization. J Biomed Mater Res 41,422–430 (1998). [PubMed: 9659612]
28. Wu Y, Puperi DS, Grande-Allen KJ & West JL Ascorbic acid promotes extracellular matrix deposition while preserving valve interstitial cell quiescence within 3D hydrogel scaffolds. J Tissue Eng Regen Med, doi:10.1002/term.2093 (2015).
29. Rider P, Kacarevic ZP, Alkildani S, Retnasingh S & Barbeck M Bioprinting of tissue engineering scaffolds. J Tissue Eng 9 (2018).
30. Cui XF, Breitenkamp K, Finn MG, Lotz M & D'Lima DD Direct Human Cartilage Repair Using Three-Dimensional Bioprinting Technology. Tissue Eng Pt A 18, 1304–1312 (2012).
31. Buckley CT, Thorpe SD, O'Brien FJ, Robinson AJ & Kelly DJ The effect of concentration, thermal history and cell seeding density on the initial mechanical properties of agarose hydrogels. J Mech Behav Biomed 2, 512–521 (2009).
32. Yang PJ, Levenston ME & Temenoff JS Modulation of mesenchymal stem cell shape in enzyme-sensitive hydrogels is decoupled from upregulation of fibroblast markers under cyclic tension. Tissue Eng Part A 18, 2365–2375, doi:10.1089/ten.TEA.2011.0727 (2012). [PubMed: 22703182]
33. Kluin J et al. In situ heart valve tissue engineering using a bioresorbable elastomeric implant - From material design to 12 months follow-up in sheep. Biomaterials 125, 101–117, doi:10.1016/j.biomaterials.2017.02.007 (2017). [PubMed: 28253994]

34. Gottlieb D et al. In vivo monitoring of function of autologous engineered pulmonary valve. J Thorac Cardiov Sur 139, 723–731, doi:10.1016/j.jtcvs.2009.11.006 (2010).

35. Driessen-Mol A et al. Transcatheter implantation of homologous “off-the-shelf” tissue-engineered heart valves with self-repair capacity: long-term functionality and rapid in vivo remodeling in sheep. J Am Coll Cardiol 63, 1320–1329, doi:10.1016/j.jacc.2013.09.082 (2014) [PubMed: 24361320]

36. Syedain Z et al. 6-month aortic valve implantation of an off-the-shelf tissue-engineered valve in sheep. Biomaterials 73, 175–184, doi:10.1016/j.biomaterials.2015.09.016 (2015). [PubMed: 26409002]

37. Laske A et al. Pressure gradients across bileaflet aortic valves by direct measurement and echocardiography. Ann Thorac Surg 61, 48–57, doi:10.1016/0003-4975(95)00922-1 (1996). [PubMed: 8561632]

38. Emery RW & Nicoloff DM St. Jude Medical cardiac valve prosthesis: in vitro studies. J Thorac Cardiovasc Surg 78, 269–276 (1979). [PubMed: 459535]

39. Baumgartner H, Khan S, DeRobertis M, Czer L & Maurer G Discrepancies between Doppler and catheter gradients in aortic prosthetic valves in vitro. A manifestation of localized gradients and pressure recovery. Circulation 82, 1467–1475, doi: 10.1161/01.cir.82.4.1467 (1990). [PubMed: 2401075]

40. Yoganathan Ajit P., P. a. V. R in Practice of Clinical Echocardiography Fifth Edition (ed Otto Catherine M.) Ch. 23, 433–454 (Elsevier, 2017).

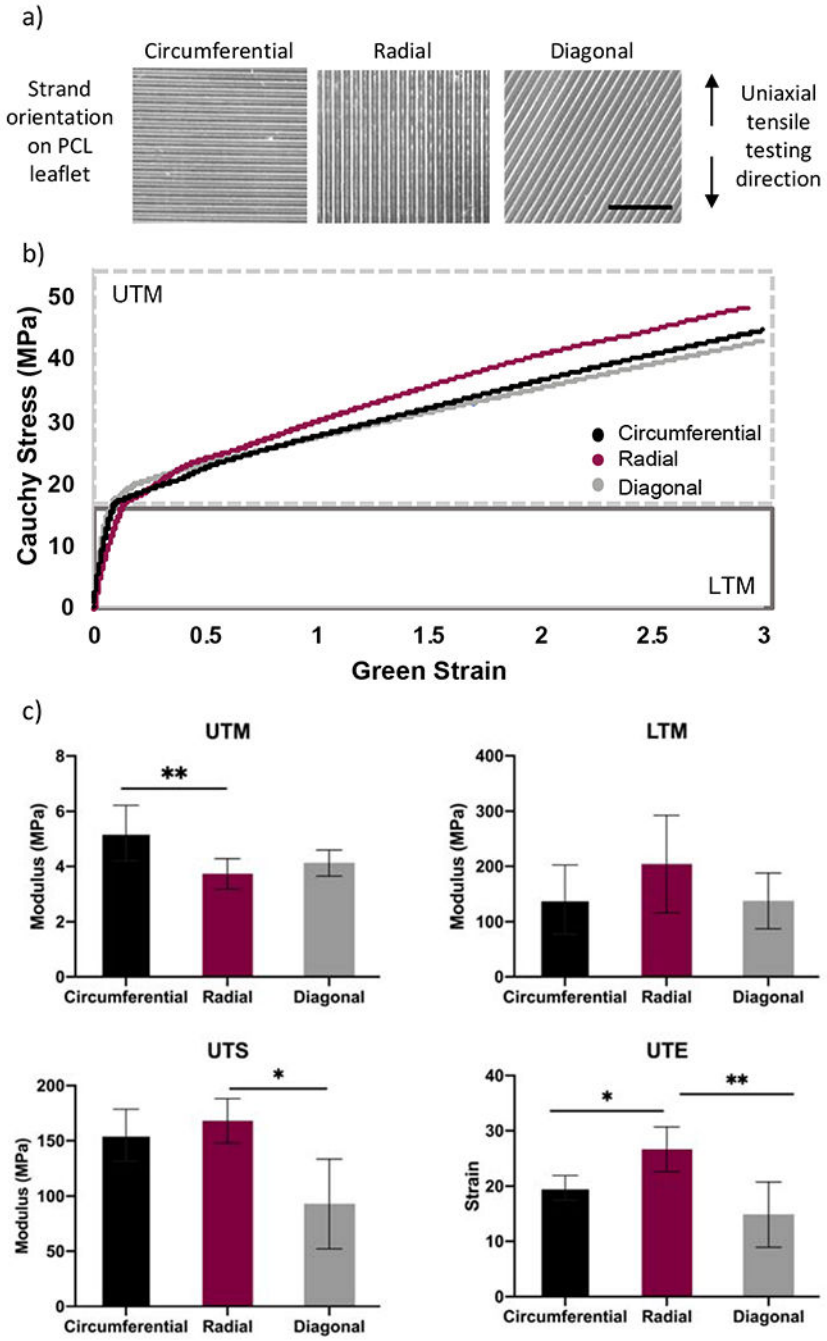

Figure 1. Mechanical properties of PCL scaffolds of three different fiber orientation.

A) Representative images of the fiber orientation of 3D printed PCL scaffolds used for tensile testing. The direction in which samples were subjected to tensile testing is demonstrated on the right. B) Representative Cauchy-Green stress-strain curve for the perpendicular, parallel, and diagonal scaffolds, where the moduli for PCL scaffolds was calculated from two different regions, the upper and the lower tangent modulus (UTM and LTM). C) The mechanical properties of the PCL scaffolds were characterized by four

properties the UTM, LTM, ultimate tensile strength (UTS), and ultimate tensile strain (UTE). N = 4. Scale bar = 5 mm. One-way ANOVA; *p<0.05; ** p<0.01; ***p<0.001.

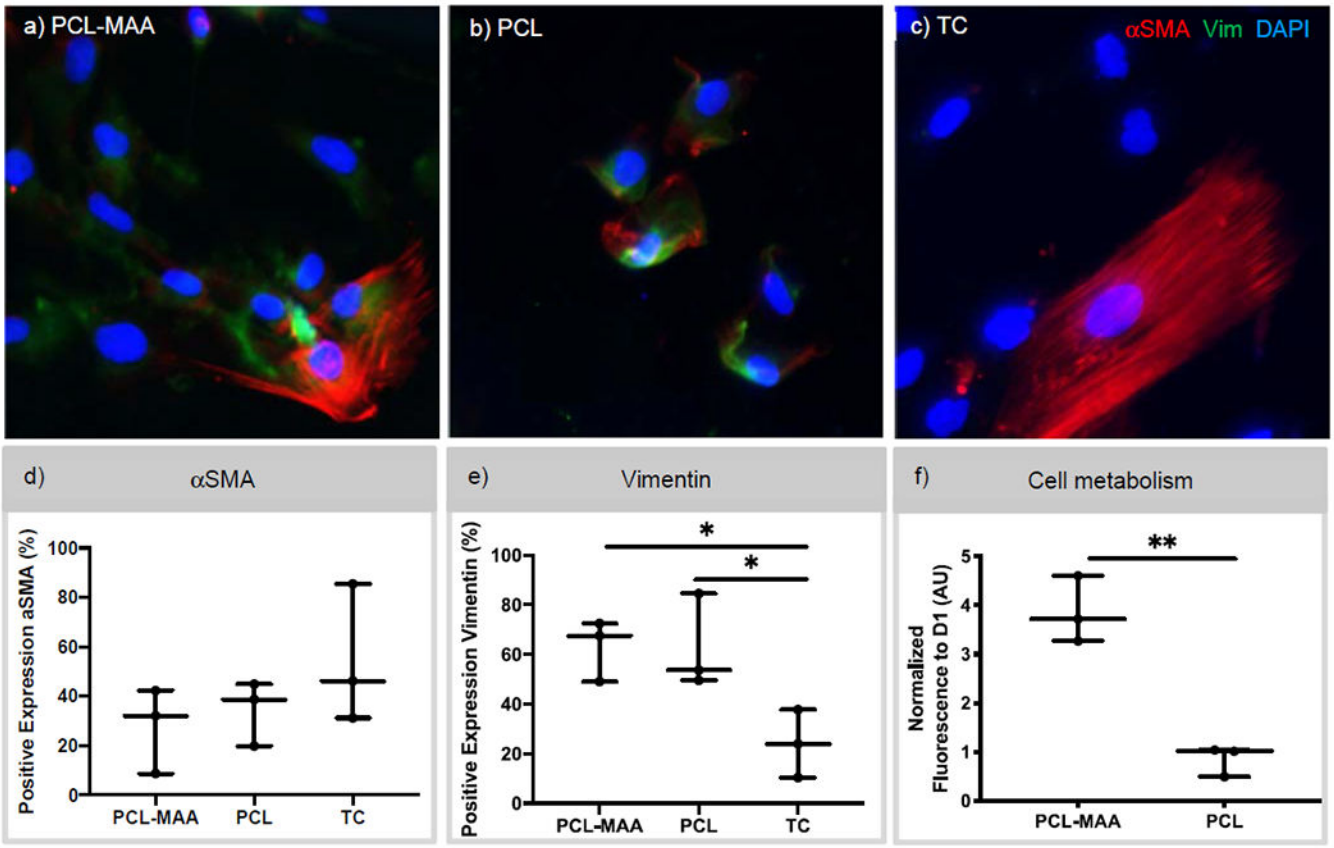

Figure 2. Characterization of cell metabolism and αSMA and vimentin expression of iMSCs when seeded on PCL-MAA and PCL.

a-c) Immunostaining of αSMA and vimentin expression of iMSCs seeded on PCL-MAA, PCL, and tissue culture (TC) after 7 days. d,e) The percentage of cells that stained positive for αSMA and vimentin was quantified from immunostaining images using CellProfiler software and a one-way ANOVA used. N = 3. DAPI – blue, vimentin – green, and αSMA – red. Scale bar 50 mm. f) Cell metabolism of iMSCs seeded on PCL-MAA and PCL scaffolds was determined via alamarBlue assay. The level of fluorescence for cell metabolism was normalized to D1 and an unpaired t-test was used for statistical analysis. N=3. *$p<0.05$; **$p<0.01$.

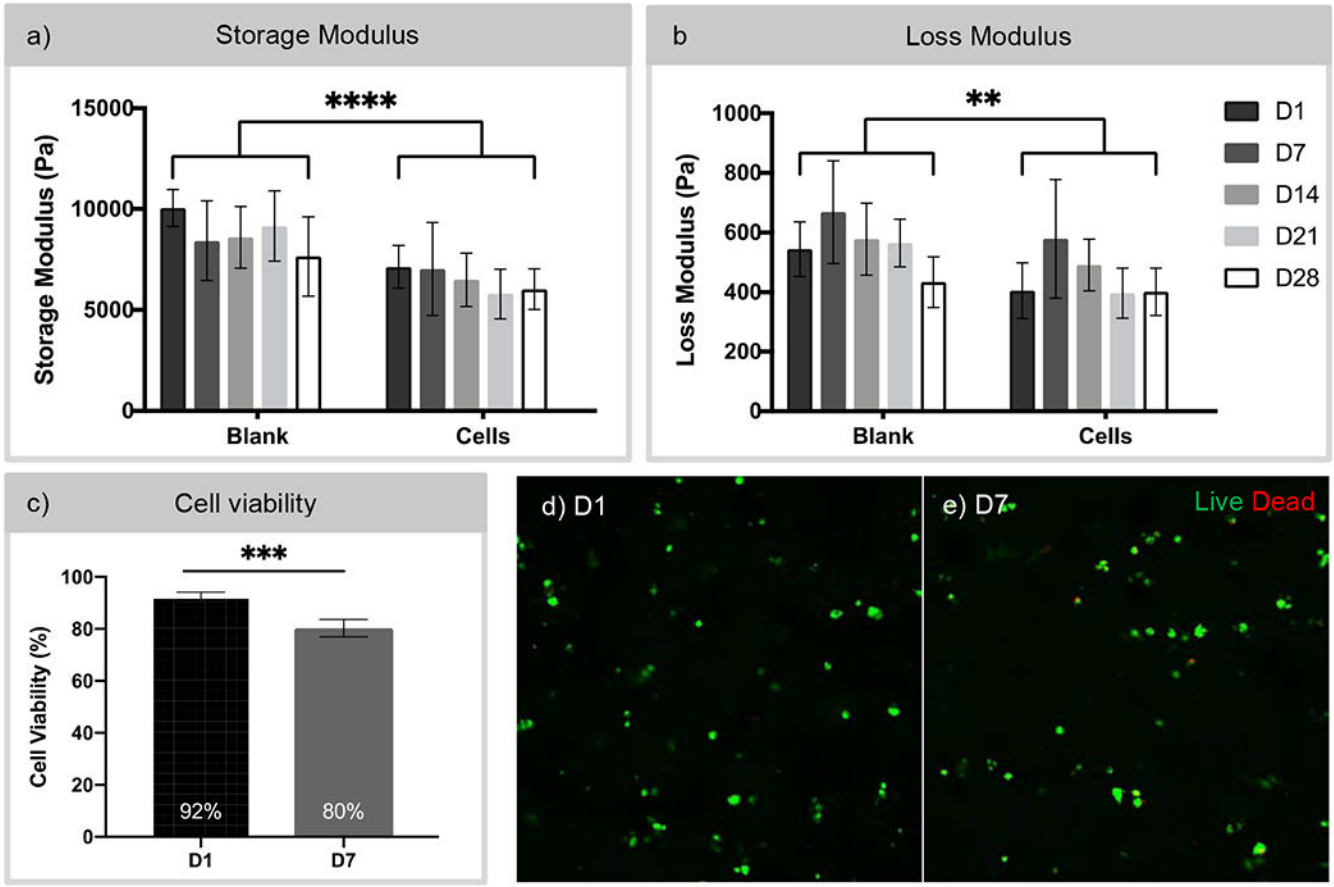

Figure 3. Characterization of the rheological and cell viability property of GelMA/PEGDA hydrogels.

a,b) Storage and loss moduli of blank GelMA/PEGDA hydrogels and GelMA/PEGDA hydrogels with encapsulated cells over 28 days measured by rheology. N = 5-6. Two-way ANOVA comparing Blank vs. Cells. ** $p < 0.001$, **** $p < 0.0001$. c) Assessment of cell viability of iMSCs encapsulated in GelMA/PEGDA hydrogels at day 1 and day 7 using the Live/Dead assay. Cell viability decreased from 92% to 80% over 7 days. However, cells remained viable within the hydrogels up to 7 days. Paired t-test, *** $p < 0.001$. d,e) Confocal imaging of cell-laden hydrogels at D1 and D7 post-encapsulation. Live – Calcein AM (green) and dead - ethidium homodimer (red). Scale bar 50 μm.

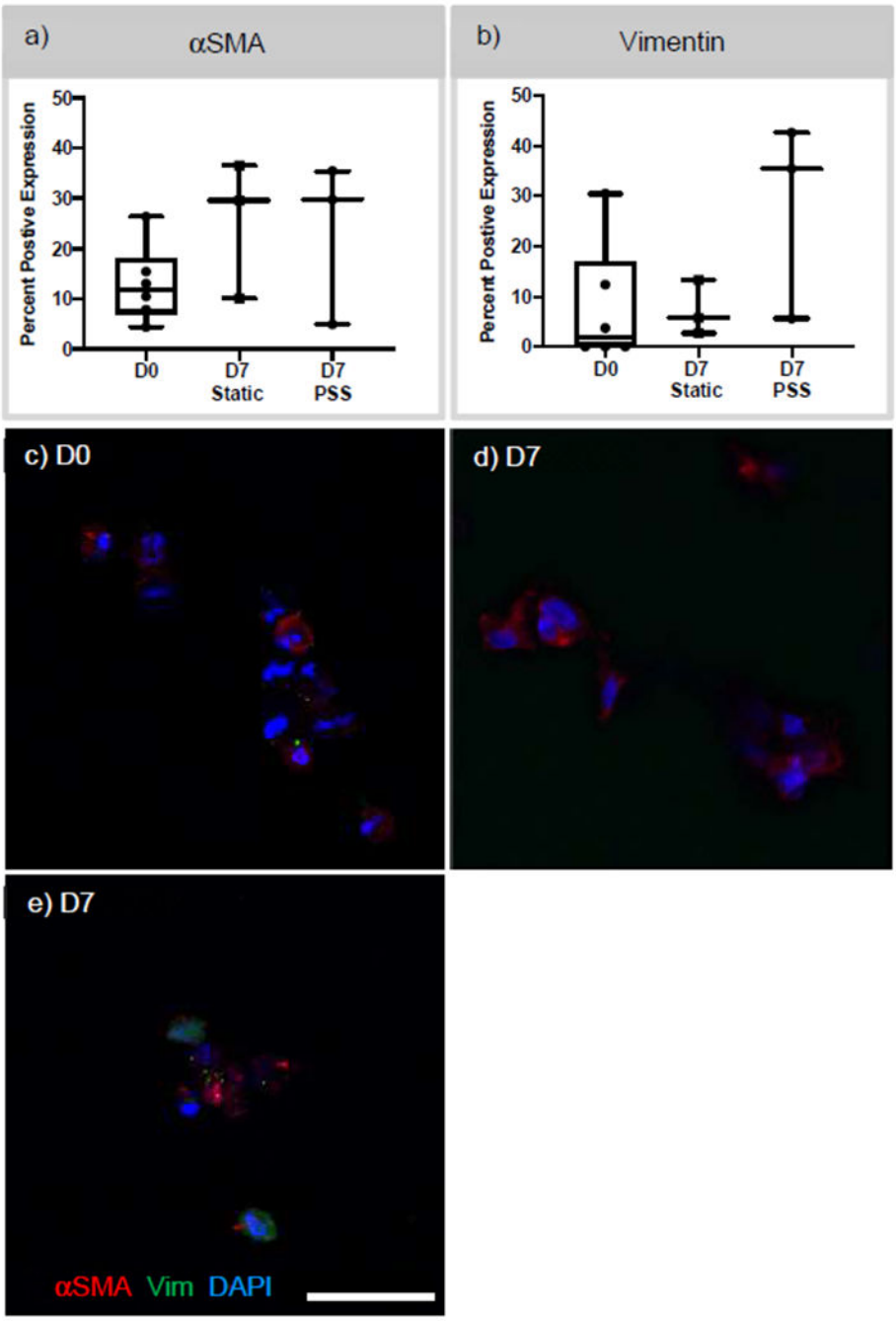

Figure 4. Characterization of αSMA and vimentin expression in cell-laden multilayered scaffolds.

a,b) αSMA and vimentin expression was quantified by determining the number of positive cells with αSMA and vimentin expression at D0 and post-D7 in static and PSS conditions. c,d,e) Confocal images of immunostaining of αSMA and vimentin at D0 and D7 PSS. N ≥ 3. Scare bar 25 μm. DAPI – blue, αSMA – Red, and vimentin – Green.

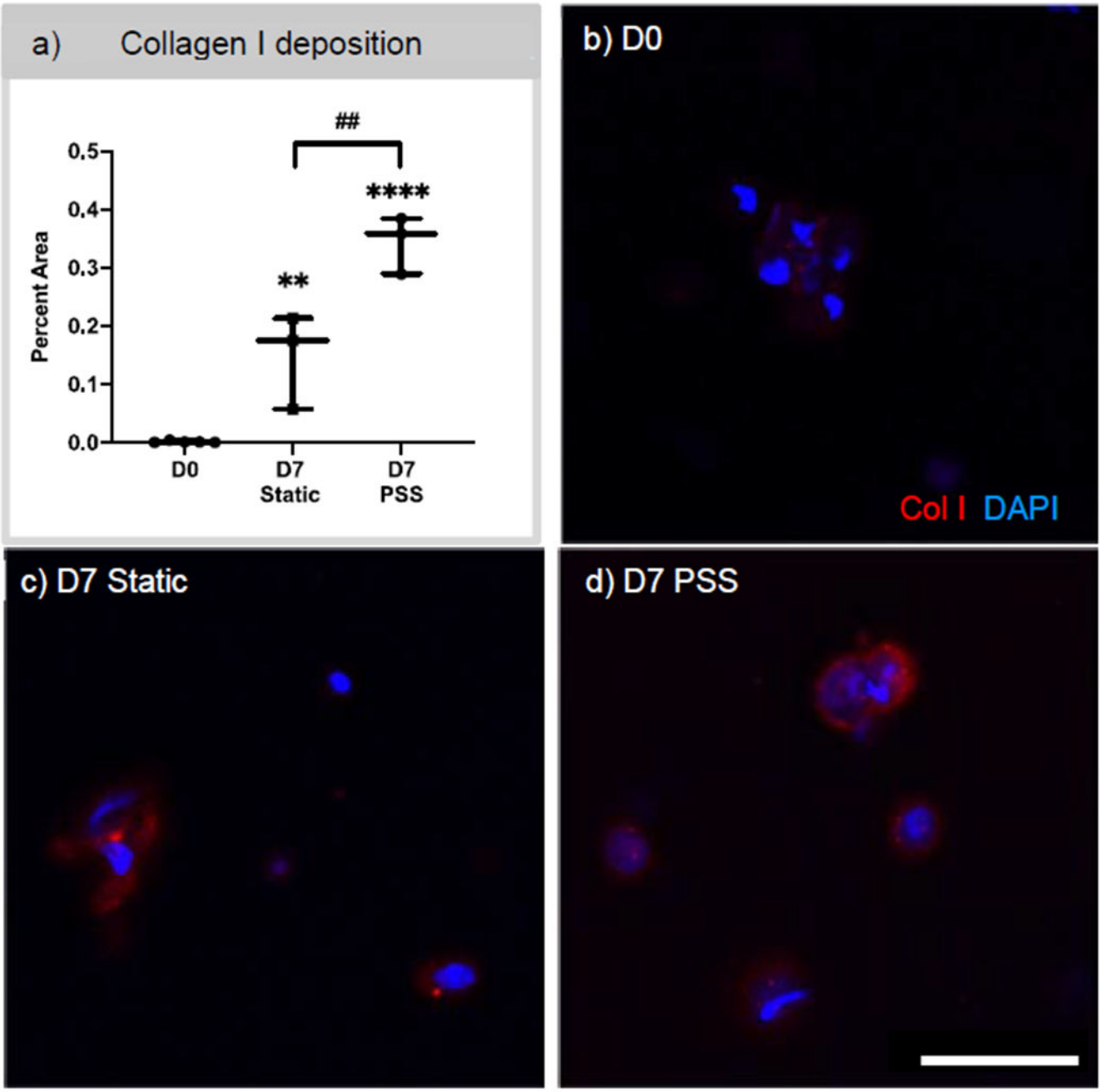

Figure 5. Quantification of collagen type I deposits in cell-laden multilayered scaffolds at day 0 and 7 under static or pulsatile shear stress (PSS) conditions.

a) Collagen type I was quantified by determining the percent area of collagen type I staining over the area of total image. One-way ANOVA was performed. b,c,d) Confocal images of immunostaining of collagen type I at D0 and D7 in either static or PSS conditions, respectively. N ≥ 3. Ordinary one-way ANOVA with post hoc Holm-Sidak's multiple comparison test. D7 samples were compared to D0 where **p<0.01; ****p<0.0001. ## p<0.01 used to compared between D7 static vs. PSS conditions. Scale bar 25 μm. DAPI – blue, Collagen type I – Red.

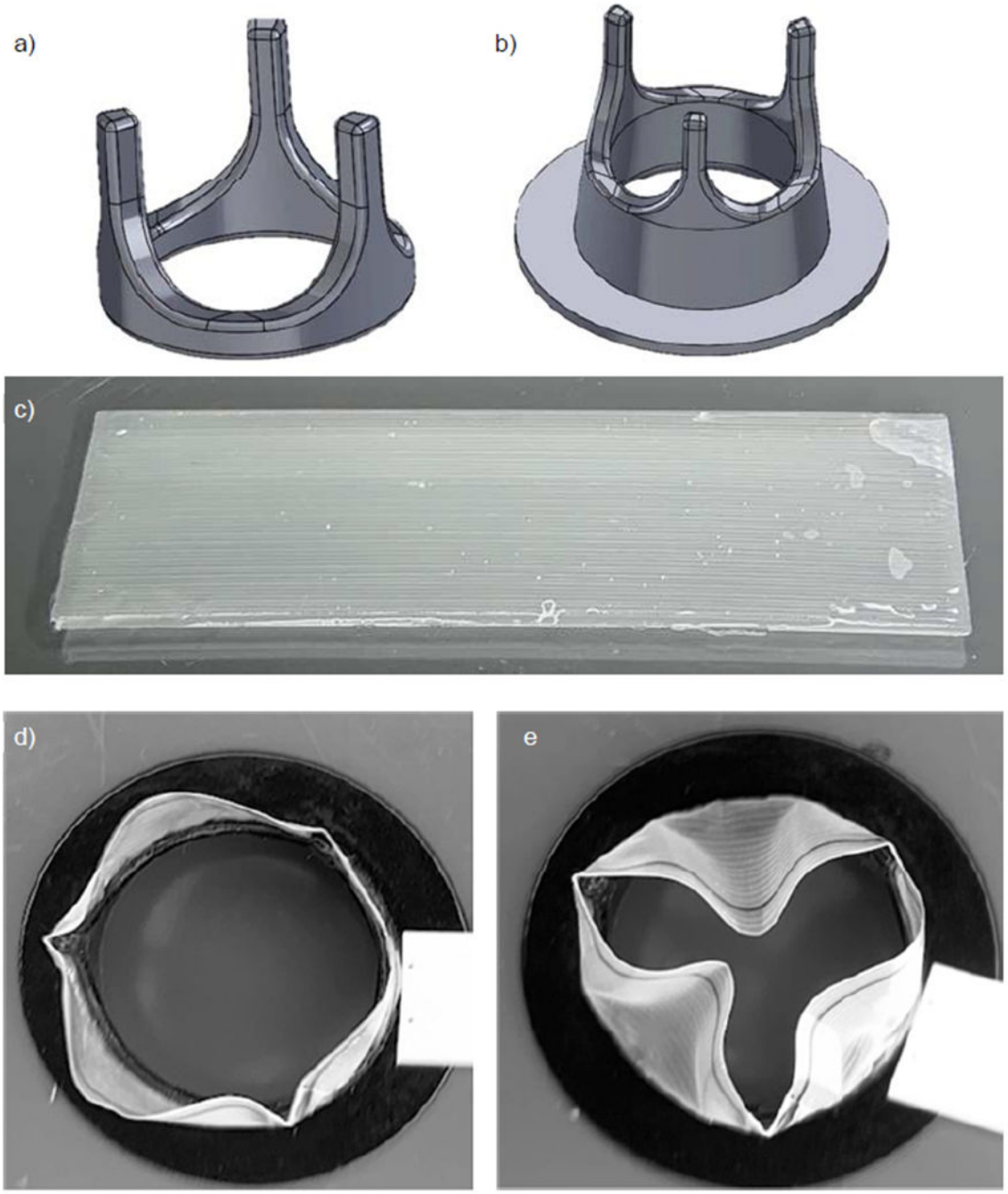

Figure 6. TEHV-PCL prototype components.

a) Valve stent of 17 mm ID and 19 OD was designed using SolidWorks. b) An additional outer diameter at the bottom of the valve stent was added to enable placement and fixation to the pulsatile flow loop. c) Image of the PCL valve leaflet with circumferential strand orientation. d, e) Completely assembled TEHV, where the leaflet was fixated to the valve stent via cyanoacrylate. Scale bar 8.5 mm.

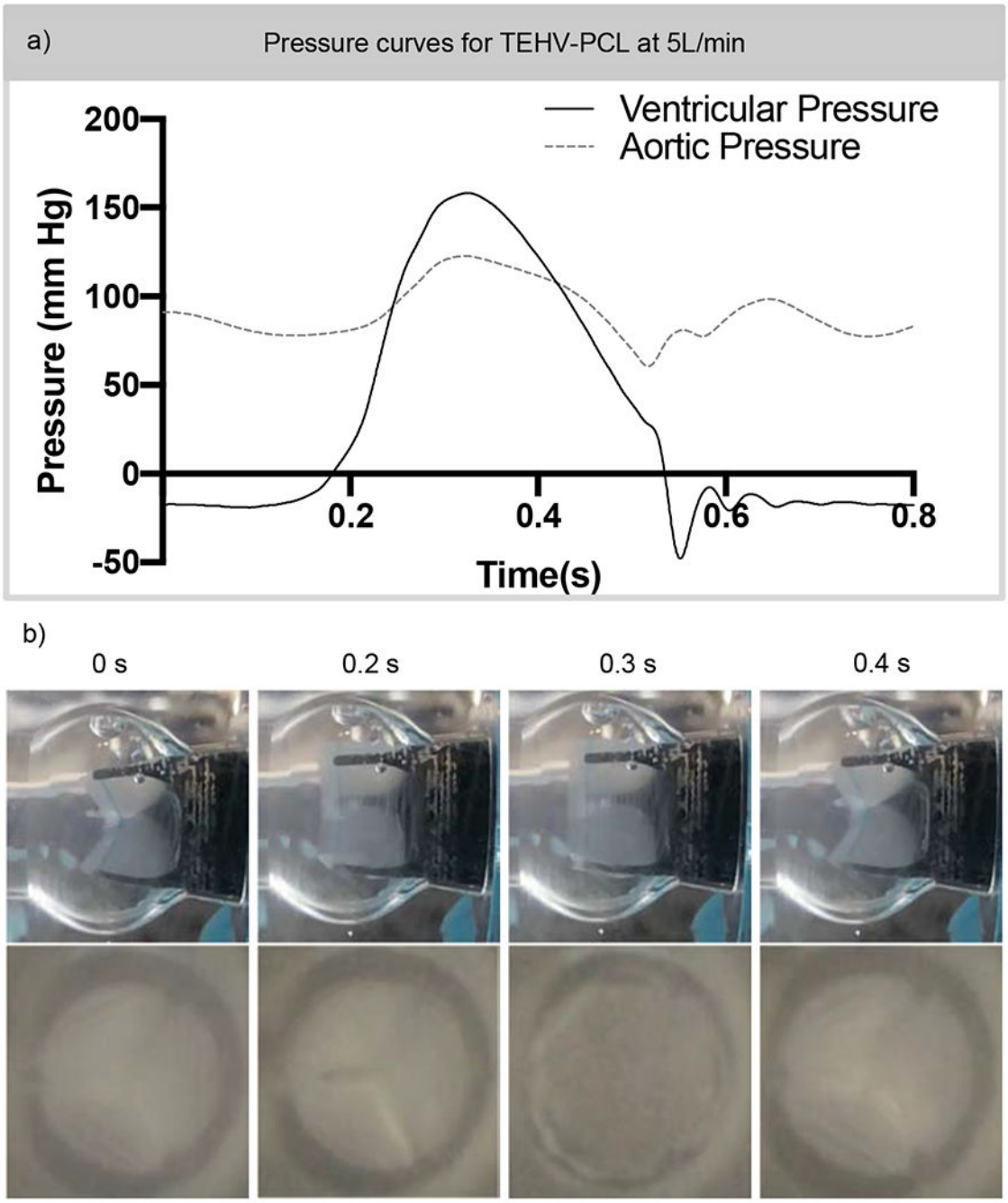

Figure 7. TEHV-PCL opening and closure during a cardiac cycle.

a) A TEHV of 19 mm OD and 17 mm ID with a 40-um thick leaflet scaffold was tested under aortic valve condition of 70 beats per minute with 5L/min output for 200 cycles. Ventricular and aortic pressures were recorded during a cardiac cycle. b) Through the transparent polycarbonate test chamber, a slow-motion video of 240 frames per second was captured and still images are displayed. The duration of the TEHV-PCL opening 0.18 ± 0.019 seconds during a cardiac cycle at 5L/min cardiac output. N = 4. Scale bar 8.5 mm.

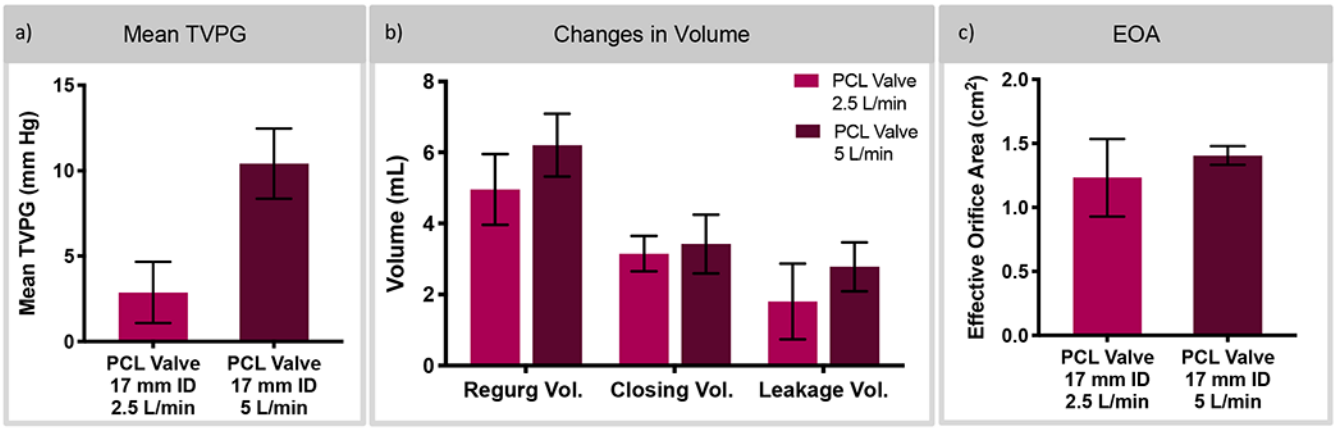

Figure 8. Evaluation of TEHV-PCL performance under pulsatile flow conditions.

PCL valves assembled using rectangular leaflet and cyanoacrylate fixation were placed into a pulsatile flow loop mimicking the left ventricular circulation by controlling the ventricular and aortic pressures. a) The mean transvalvular pressure gradient (TVPG) of the PCL valve was 2.8 mm Hg and 10.4 mm Hg for 2.5 and 5 L/min cardiac outputs, respectively. b) At both the cardiac outputs, there was minimal regurgitation, closing, and leakage volume. c) The average effective orifice area (EOA) of the TEHV-PCL was 1.23 cm^2 and 1.41 cm^2 at 2.5- and 5 L/min cardiac output. N =3-4.